Spatiotemporal Spin Noise Spectroscopy

Steeve Cronenberger, Chahine Abbas, Denis Scalbert, H. Boukari

Spatiotemporal Spin Noise Spectroscopy

S. Cronenberger, C. Abbas, and D. Scalbert
Laboratoire Charles Coulomb (L2C), UMR 5221 CNRS-Université de Montpellier, Montpellier FR-34095, France

H. Boukari
Université Grenoble Alpes, F-38000 Grenoble, France and CNRS, Institut NEEL, Grenoble F-38000, France

(Received 9 April 2019; published 2 July 2019)

We report on the potential of a new spin noise spectroscopy approach by demonstrating all-optical probing of spatiotemporal spin fluctuations. This is achieved by homodyne mixing of a spatially phase-modulated local oscillator with spin-flip scattered light, from which the frequency and wave vector dependence of the spin noise power is unveiled. As a first application of the method we measure the spatiotemporal spin noise in weakly n-doped CdTe layers, from which the electron spin diffusion constant and spin relaxation rates are determined. The absence of spatial spin correlations is also shown for this particular system.

DOI: 10.1103/PhysRevLett.123.017401

Direct measurement of spin fluctuations by an optical spin noise technique is becoming the mainstream approach for noninvasive studies of spin dynamics in complex atomic and condensed matter systems [1–3]. Recent progress in experimental methods make this approach quite promising to explore many exciting problems at the frontier of atomic [4] and condensed matter physics [5,6]. Noteworthy experimental developments include broadband spin noise spectroscopy (SNS) using pulsed lasers [7,8], heterodyne detection [9], cross-correlation spectroscopy [10], two-color SNS [11], and SNS beyond second-order spin correlators [12,13].

However, the difficulty to extract the weak spin noise from other noise sources, particularly in condensed matter, is often overcome by increasing the optical power used to probe the sample. This questions the noninvasive character of SNS. This problem has been partly solved by the heterodyne and homodyne detection, which permits us to raise the optical level above the noise equivalent power of the detector, while keeping a low probe power to investigate the sample [9,14,15].

Notwithstanding these numerous technical advances, current SNS only addresses time spin correlations, at the expense of spatial correlations. Thus, valuable information on spin transport or many-body spin interactions is missed. Two-beam spin noise arrangements have been proposed to test spin transport and spin diffusion but without proof of concept [16,17].

In standard SNS, the spin fluctuations in the sample are probed, through the Faraday effect, by a linearly polarized laser propagating in the z direction [1,18,19]. The rotation angle of the direction of polarization is a weighted average of the spin fluctuations over the laser spot, so that all spatial information is irremediably lost. However, spin induced Faraday rotation and spin-flip Raman scattering (SFRS) are known to be intimately related phenomena, because they result from the same spin-dependent term in the dielectric polarization [20–22]. Therefore SNS can be described either as Faraday noise, or as interference of forward-scattered Raman light with the transmitted probe [2,23]. In this spirit, SNS differs from SFRS by the method of measurement only [2]. In SFRS wave vector selective detection of spin excitations can be achieved by an appropriate choice of the incident and scattered photon wave vectors. This suggests that selective wave vector detection of spin fluctuations should be feasible in SNS by selecting appropriate scattered photons through homodyne detection.

In homodyne or heterodyne detection of spin noise, the transmitted probe beam is blocked by a cross polarizer to suppress the Faraday noise. As the Raman scattered light is crossed polarized, it propagates to the detector, where it is mixed with a reference beam [the local oscillator (LO)]. The optical mixing converts the optical frequencies contained in the SFRS spectrum into the radio frequency domain [2], and can then be detected with a high bandwidth optical detector [9,14,15].

In this Letter we show that a complete picture of spatiotemporal spin fluctuations can be retrieved with a single spatially uniform probe beam interacting with the sample. It must be noted that the image of the SFRS field formed on the detector is a faithful copy of the spatial spin fluctuation pattern in the sample at a given time. The idea is then to amplify selectively the part of the image field where the spatial spin fluctuation is encoded. This can be achieved by optical mixing with a judiciously chosen intensity and phase-controlled reference field. As an example, one can spatially resolve the spin noise signal by optical mixing

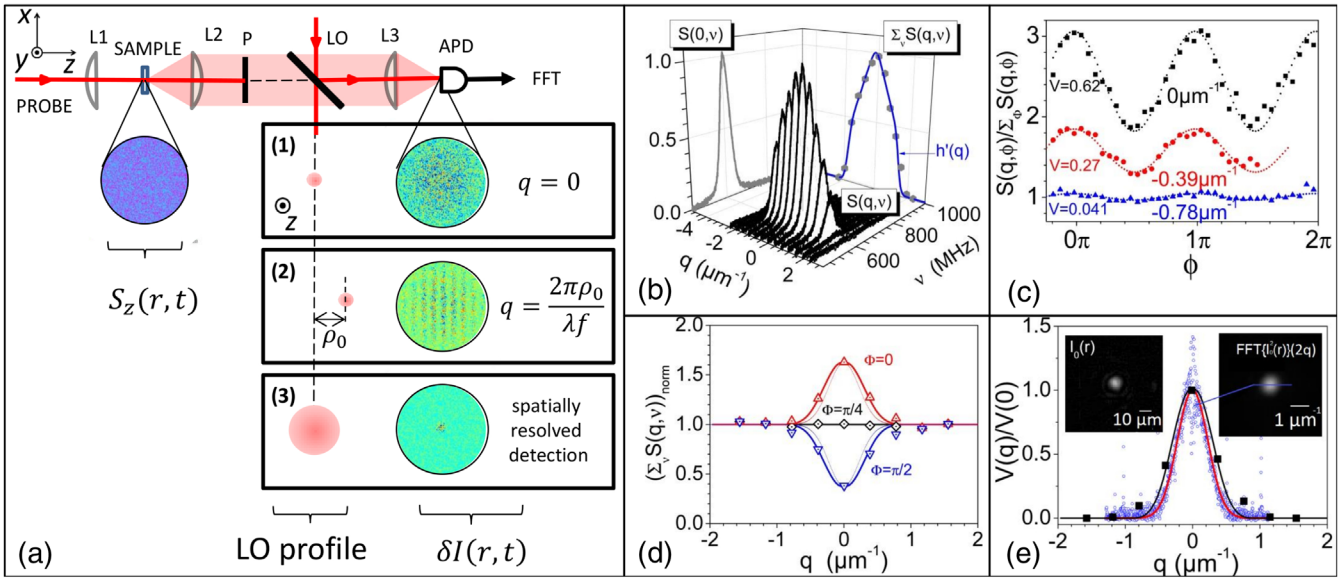

FIG. 1. (a) Principle of detection of the spatiotemporal spin fluctuations by homodyne mixing of the spin-flip Raman scattered light with a phase-controlled local oscillator (the details of the experimental setup are given in the Supplemental Material [24]). A linearly polarized probe beam interacts with the sample, and a linear polarizer P, cross polarized with respect to the probe, selects the light scattered by the spatiotemporal spin fluctuation $S_z(r,t)$. The scattered light is imaged on an avalanche photodiode (APD), where it is mixed with the LO field. Three cases are illustrated as follows: panels 1–2 show q-selective detection of spin noise at $q=0$ (LO with a constant phase in panel 1), or at $q\neq 0$ (LO with a linear spatial phase shift in panel 2), and panel 3 shows tightly focused LO (spatially resolved detection). (b) 3D plot of the noise power $S(q,\nu)$ measured on sample A at $T=5.2$ K with 1 mW probe power. The frequency integrated noise power (dots) is compared with $h'(q)$ (blue curve), which is the convolution of the calculated optical transfer function $h(q)$ with $\hat{I}_0^2(q)$ (see text). The spin noise spectrum at $q=0$ is also shown. The data in panels (c)–(e) were obtained with sample B. (c) Integrated noise power $S(q,\phi)$ measured vs ϕ (actively stabilized) for different q. The curves are vertically offset for clarity. (d) Normalized integrated noise power $S(q,\phi)/h'(q)$ vs q for different ϕ [triangles are the experimental points, the dotted lines are calculated with Eq. (2), and the solid lines are calculated with Eq. (1)]. (e) Visibility $V(q)$ obtained from data in (d) (symbols), compared to the theoretical values calculated from the measured profile with Eq. (1) (black curve) and Eq. (2) (red curve).

with a strongly focused LO beam [panel (3) of Fig. 1(a)]. It is also possible to probe spatial spin correlations by monitoring the cross-correlation of the intensity noise from two detectors, and two LO focused at different positions on the image. Here we choose to amplify selectively Fourier components of the spatial spin correlations with a controllable spatial frequency q.

The experimental approach is illustrated in panels 1–2 of Fig. 1(a). The spatial frequency is controlled by shifting the LO from the probe by a distance $\boldsymbol{\rho}_0$. Homodyne mixing amplifies selectively the spin fluctuations with wave vector $q=2\pi\boldsymbol{\rho}_0/\lambda f$, where λ is the photon wavelength, and f the focal length of L3. For Gaussian beams, and in the 2D case, the measured spin-related intensity noise power can be expressed as [24]

$$S(q,\nu,\phi)=[(h\hat{K})\otimes\hat{I}_0^2]_q+\cos(2\phi)[\hat{I}_0^2]_q[(h\hat{K})\otimes\hat{I}_0^2]_0, \tag{1}$$

where $h(q)$ is the optical transfer function of the imaging system between the sample and the detector, $\hat{K}(q,\nu)$ is the wave vector and frequency dependent spin noise power, $I_0(r)$ is the intensity of the probe spot on the sample with $\hat{I}_0(q)$ its Fourier transform, and ϕ is the relative phase between the LO and the probe, which may be actively stabilized or not. $h(q)$ is merely the Fourier transform of the point spread function of the optical system with finite spatial resolution. As a result, high-spatial frequencies in the noise spectrum are cut. The convolutions in Eq. (1) take into account the finite resolution in q due to the finite size of the probe spot on the sample. There is a wave vector dependent contribution, and a $q=0$ contribution weighted by $\hat{I}_0^2(q)$, meaning that it is present only when the probe and the LO beams overlap.

For large spots the following approximate equation can be used (see Supplemental Material [24])

$$S(q,\nu,\phi)=h(q)\hat{K}(q,\nu)\left(1+\cos(2\phi)\frac{\hat{I}_0^2(2q)}{\hat{I}_0^2(0)}\right). \tag{2}$$

Experimental tests of Eq. (1) were performed using two n-doped CdTe layers grown by molecular beam epitaxy. Sample A is 500 nm thick aluminium doped CdTe layer, with an electron density of about 2×10^{17} cm^{-3}, grown on CdTe(100). It was used for experiments in reflection geometry. Sample B is a 10 μm thick aluminium doped

CdTe layer, with electron density of about 2×10^{16} cm^{-3}, grown on $Cd_{0.96}Zn_{0.04}Te(100)$. Sample B allows for measurements in a transmission geometry. In reflection experiments the probe wavelength corresponds to the resonance on the exciton bound to the neutral donor while it is shifted 10 meV below for transmission experiments (see Supplemental Material [24] for details of the setup).

We first demonstrate the effect of $h(q)$ on the measured noise power by intentionally modulating ϕ to average out the term related to the spatial coherence [Fig. 1(b)]. Using Eq. (1) the noise spectrum becomes

$$S(q,\nu) = [(h\hat{K}) \otimes \hat{I}_0^2]_q. \tag{3}$$

If one assumes that there are no spatial spin correlations then one can easily demonstrate that the integrated spin noise obeys the sum rule $\sum_\nu \hat{K}(\mathbf{q},\nu) = \langle S_z^2 \rangle$, and therefore $\sum_\nu S(q,\nu) = \langle S_z^2 \rangle [h(q) \otimes \hat{I}_0^2(q)] = \langle S_z^2 \rangle h'(q)$. The proportionality between the integrated spin noise power and the calculated $h'(q)$ evidenced in Fig. 1(b) confirms the absence of spatial spin correlations. In order to estimate the smallest measurable spin correlation length ξ we simulated the effect of a correlation function of the form $K(\mathbf{r}) = e^{-|\mathbf{r}|/\xi}$. Figure 2 compares the integrated noise power calculated with Eq. (3) and the measurement taken from Fig. 1(b). The agreement between experiment and theory is very good for $K(r) = \delta(r)$ (no spatial correlations), and degrades for $\xi = q_c^{-1} = 0.313$ μm, where $q_c = 2\pi(D/\lambda f)$ is the wave vector cutoff of the objective collecting the scattered field, and D is the optical aperture of the objective. One can conclude that the method can resolve $\xi \geq q_c^{-1}$, while a system with $\xi \leq (2q_c)^{-1}$ will appear as uncorrelated.

Then we stabilize the phase ϕ in order to explore the effect of the beam coherence (See Supplemental Material [24] for phase stabilization). Because of vibrations of the sample in the cryostat, stabilization of the phase could be done only in transmission geometry. Therefore we used sample B for these experiments. Figure 1(c) shows the oscillations of the integrated spin noise power with ϕ, as a result of the coherent mixing between the LO and the probe. As expected from Eqs. (1)–(2), the amplitude of the oscillations decreases as q increases. This is quantified by the visibility of the oscillations defined as $V(q) = [S_i(q,0) - S_i(q,\pi/2)]/[S_i(q,0) + S_i(q,\pi/2)]$, where $S_i(q,\phi) = \sum_\nu S(q,\nu,\phi)$. Figure 1(d) shows that in agreement with Eqs. (1)–(2) the integrated noise power normalized by $h'(q)$ is flat for $\phi = \pi/4$ due to the absence of long-range spatial correlations, and exhibits either a peak ($\phi = 0$) or a dip ($\phi = \pi/2$) at $q = 0$. These structures are better described by the exact expression in Eq. (1), which takes into account the convolution with $\hat{I}_0^2(q)$. Finally, in Fig. 1(e) we compare the measured visibility $V(q)$ and the one calculated either with Eq. (1) or Eq. (2). Again we have a good agreement except at $q = 0$, where the measured visibility is significantly lower than 1. This can be caused by an eventual distortion of the probe wave front by the sample, whose back face has been mechanically polished.

As explained above, we have established the spatiotemporal homodyne spin noise spectroscopy technique that is limited by the finite optical resolution of the setup and the wave vector distributions of the beams.

As a first application of the method we study the spatiotemporal electron spin fluctuations in sample B. In these experiments ϕ was modulated in order to remove the coherence term of Eq. (1) so that Eq. (3) can be used to interpret the data. This means that there is a direct correspondence between the measured noise and the spin noise at the same q. Figure 3 illustrates the dispersion of the spin noise spectra with q in a transverse magnetic field. The

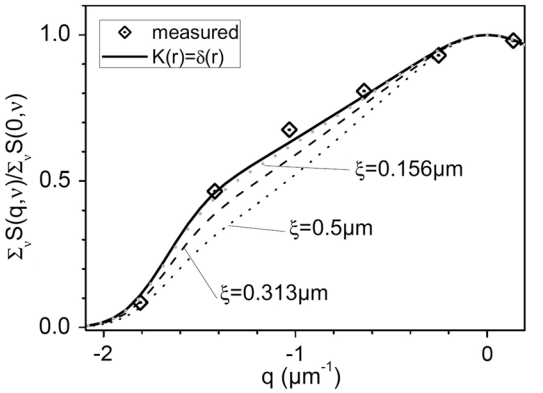

FIG. 2. Wave vector dependence of the integrated spin noise power spectra (symbols) compared to frequency integrated spin noise power calculated with Eq. (3), for no spatial correlations (solid line) and correlations with a spatial extent ξ (dashed and dotted lines).

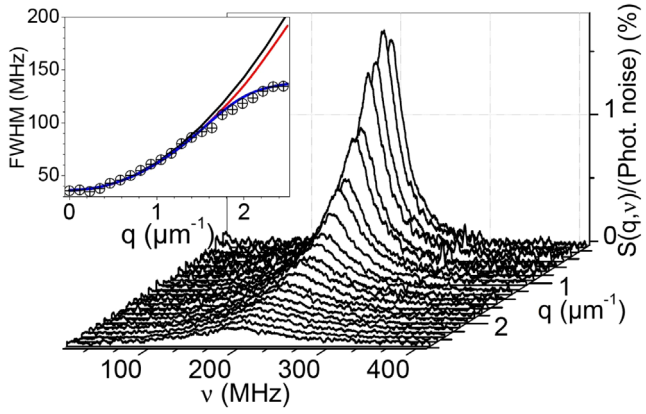

FIG. 3. Waterfall plot of spin noise spectra measured for a series of q vectors in transmission geometry on sample B (4.1 K, 1.1 mW). The inset shows the FWHM vs q deduced from Lorentzian fits to the noise spectra. The black curve is a quadratic fit to the data for small q. The red curve takes into account the finite wave vector resolution. The blue curve takes into account the wave vector cutoff effect.

spin noise line is centered on the Larmor frequency consistent with the electron g factor $g_e = -1.65$, and we do not detect any frequency shift with q. This corroborates the idea that there are no collective spin excitations in this system. However a strong broadening of the noise spectrum is evidenced, which is first quadratic for small q, and then levels off (see inset of Fig. 3). We interpret the quadratic broadening as a consequence of electron spin diffusion. Indeed in the absence of spatial correlations, the decay of a spatially modulated spin fluctuation proceeds via two independent mechanisms: the electron spin relaxation and spin diffusion. This can be seen as a direct consequence of the fluctuation-dissipation theorem, which relates $\hat{K}(q,\nu)$ to the imaginary part of the complex susceptibility $\chi(q,\nu)$. A simple calculation of the susceptibility from the Bloch equations in the presence of spin diffusion gives $\chi(q,\nu) \propto [2\pi(\nu-\nu_L) + i(\gamma_s + D_s q^2)]^{-1}$, where D_s is the spin diffusion coefficient, γ_s is the spin relaxation rate, and ν_L is the Larmor frequency. The discrepancy from quadratic broadening at larger q is due to the wave vector cutoff effect (see Sec. II-C of the Supplemental Material [24]), as confirmed by the calculation. The LO can be shifted away from the optical axis to increase the range of q not affected by the wave vector cutoff. We also checked that the finite wave vector resolution does not significantly influence the measured values of D_s and γ_s [compare red and black curves in Fig. (3)]. We see that we get the same information as in the transient spin grating technique [27,28], without need to excite the sample, nor to change the conditions of illumination of the sample, simply by monitoring the decay of the spontaneous spatiotemporal spin fluctuations imaged on the detector.

Finally, we measured the spatiotemporal spin dynamics as a function of temperature. The damping rate is obtained by fitting the spin noise spectra with a Lorentzian. Figure 4(a) shows that γ increases quadratically with q as

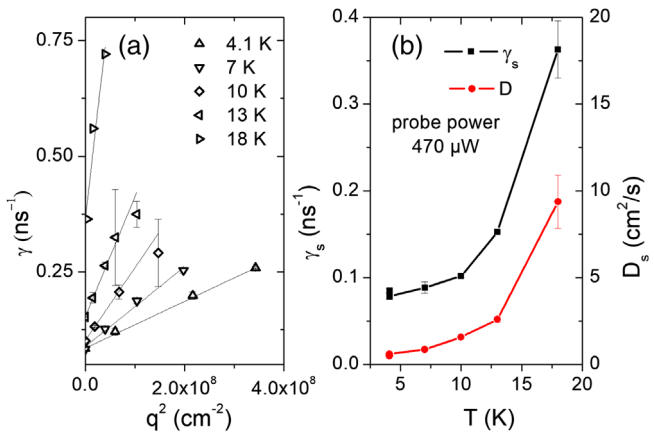

FIG. 4. (a) Damping rate γ vs q^2 for a series of temperatures (symbols, data; solid lines, linear fits of the data). (b) Relaxation rate γ_s at $q = 0$, and spin diffusion coefficient D_s deduced from the linear fits shown in the left panel.

expected in the presence of spin diffusion (here the pupil effect has been avoided). Figure 4(b) shows the temperature dependence of the spin relaxation rate γ_s, and the spin diffusion constant D_s obtained by fitting the data with $\gamma(q) = \gamma_s + D_s q^2$. Both γ_s and D_s increase rapidly with temperature. Unfortunately, data from literature on electron spin relaxation and spin diffusion in bulk CdTe, to which our data should be compared, are scarce [29]. Nevertheless one can tentatively interpret our results using the well-established spin relaxation mechanisms identified in bulk GaAs [30,31]. At low temperature and low electron densities, the electron spin relaxation is mainly caused by the fluctuating nuclear fields, and by the anisotropic exchange interaction (AEI) between donors [32]. In our sample the donor density is about 10 times below the Mott transition, and the compensation by acceptors is probably negligible. In this case, and for low enough temperature, electrons are localized on donors. If one assumes that spin diffusion occurs mainly via spin exchange between nearest donors, then $D_s \simeq R^2/\tau_c$, where $R = \beta n^{-1/3}$ is the average characteristic distance between effectively interacting donors with $0.54 \leq \beta \leq 0.8$ [30], and τ_c is the spin correlation time on a neutral donor site. From the measured value of D_s at $T = 4.7$ K we find $\tau_c = 6.6$–14.5 ps, depending on the value β, slightly shorter than the calculated values $\tau_c^{\text{th}} = 18$–27 ps deduced from the inter-donor isotropic exchange interaction [30,33]. One cannot exclude a shortening of τ_c due to the interaction of localized electrons with free electrons [34]. This short correlation time also implies that the spin relaxation induced by the fluctuating nuclear fields is inefficient due to motional narrowing. Hence, we are left with the spin relaxation due to AEI. In order to estimate the corresponding spin relaxation rate one needs the value of the Dresselhaus coefficient γ_D [35]. Published values of γ_D for CdTe spread in the range 8.5–45 eV Å^3 [36–38]. In the absence of consensus we treat it as an adjustable parameter to reproduce $\gamma_s \simeq 0.08$ ns^{-1} measured at the lowest temperature. The obtained $\gamma_D = 18$ eV Å^3 is close to the value for GaAs [31]. Yet if spin diffusion and spin relaxation were only limited, respectively, by the isotropic and anisotropic part of the exchange interaction between donors, D_s and γ_s should be temperature independent. Although their variation starts to level off at the lowest temperatures, we do not reach a well-defined plateau [39]. This forbids a more precise determination of γ_D.

In summary, we have demonstrated that spatiotemporal electron spin dynamics can be unveiled by the spin noise spectroscopy technique. The measured spin noise spectra are thus resolved not only in frequency, but also in wave vector. This gives access to spin transport, spin diffusion, and eventual spatial spin correlations. The highlight of the technique being that all spatial resolution is realized on the detector, by optical mixing of the signal with a local oscillator with adapted spatial phase and profile. This

new approach leaves the sample minimally disturbed by a homogeneous and weakly focused probe beam. We have illustrated the technique with preliminary results obtained on the electron spin dynamics in *n*-doped CdTe layers, where spin diffusion and spin relaxation were simultaneously measured. Our method offers an interesting alternative to transient spin gratings, since there is no need to excite the sample by short optical pulses.

Beyond its interest for a full characterization of the dynamics of uncorrelated spins, this method is also very promising for studying various quantum many-body spin effects, such as the many-body localized phase predicted in disordered quantum media [40], or spatial spin correlations in interacting trapped spin-polarized condensates of polaritons in microcavities [41,42].

[1] J. Hubner, F. Berski, R. Dahbashi, and M. Oestreich, Phys. Status Solidi B **251**, 1824 (2014).
[2] M. M. Glazov and V. S. Zapasskii, Opt. Express **23**, 11713 (2015).
[3] N. A. Sinitsyn and Y. V. Pershin, Rep. Prog. Phys. **79**, 106501 (2016).
[4] F. Li, J. Ren, and N. A. Sinitsyn, Europhys. Lett. **105**, 27001 (2014).
[5] F. Li, Y. V. Pershin, V. A. Slipko, and N. A. Sinitsyn, Phys. Rev. Lett. **111**, 067201 (2013).
[6] D. Roy, R. Singh, and R. Moessner, Phys. Rev. B **92**, 180205(R) (2015).
[7] S. Starosielec and D. Hägele, Appl. Phys. Lett. **93**, 051116 (2008).
[8] G. M. Müller, M. Römer, J. Hübner, and M. Oestreich, Phys. Rev. B **81**, 121202(R) (2010).
[9] S. Cronenberger and D. Scalbert, Rev. Sci. Instrum. **87**, 093111 (2016).
[10] D. Roy, L. Yang, S. A. Crooker, and N. A. Sinitsyn, Sci. Rep. **5**, 9573 (2015).
[11] L. Yang, P. Glasenapp, A. Greilich, D. R. Yakovlev, M. Bayer, and S. A. Crooker, Nat. Commun. **5**, 4949 (2014).
[12] F. Li, A. Saxena, D. Smith, and N. A. Sinitsyn, New J. Phys. **15**, 113038 (2013).
[13] F. Li, S. A. Crooker, and N. A. Sinitsyn, Phys. Rev. A **93**, 033814 (2016).
[14] M. Y. Petrov, A. N. Kamenskii, V. S. Zapasskii, M. Bayer, and A. Greilich, Phys. Rev. B **97**, 125202 (2018).
[15] P. Sterin, J. Wiegand, J. Hübner, and M. Oestreich, Phys. Rev. Applied **9**, 034003 (2018).
[16] Y. V. Pershin, V. A. Slipko, D. Roy, and N. A. Sinitsyn, Appl. Phys. Lett. **102**, 202405 (2013).
[17] G. G. Kozlov, I. I. Ryzhov, and V. S. Zapasskii, Phys. Rev. A **97**, 013848 (2018).
[18] M. M. Glazov, *Electron and Nuclear Spin Dynamics in Semiconductor Nanostructures* (Oxford University Press, Oxford, 2018), Vol. 1.
[19] J. Hubner and M. Oestreich, in *Spin Phys. Semicond.*, Springer Series in Solid-State Sciences Vol. 157, edited by M. I. Dyakonov (Springer International Publishing, Cham, 2017).
[20] Y. Shen and N. Bloembergen, Phys. Rev. **143**, 372 (1966).
[21] P. Pershan, J. van der Ziel, and L. Malmstrom, Phys. Rev. **143**, 574 (1966).
[22] R. Romestain, S. Geschwind, and G. E. Devlin, Phys. Rev. Lett. **35**, 803 (1975).
[23] B. M. Gorbovitsky and V. I. Perel, Opt. Spektrosk. **54**, 388 (1983).
[24] See Supplemental Material at http://link.aps.org/supplemental/10.1103/PhysRevLett.123.017401 for experimental arrangement and theoretical modelling of wave vector resolved spin noise spectroscopy, which includes Refs. [25,26].
[25] J. W. Goodman, *Introduction to Fourier Optics* (Roberts and Company Publisher, Greenwood village, 2005), Vol. 3.
[26] J. C. Dainty, in *Laser Speckle and Related Phenomena*, Topics in Applied Physics Vol. 9 (Springer Berlin Heidelberg, Berlin, Heidelberg, 1975).
[27] A. R. Cameron, P. Riblet, and A. Miller, Phys. Rev. Lett. **76**, 4793 (1996).
[28] S. G. Carter, Z. Chen, and S. T. Cundiff, Phys. Rev. Lett. **97**, 136602 (2006).
[29] D. Sprinzl, P. Horodyská, N. Tesarová, E. Rozkotová, E. Belas, R. Grill, P. Malý, and P. Němec, Phys. Rev. B **82**, 153201 (2010).
[30] R. I. Dzhioev, K. V. Kavokin, V. L. Korenev, M. V. Lazarev, B. Y. Meltser, M. N. Stepanova, B. P. Zakharchenya, D. Gammon, and D. S. Katzer, Phys. Rev. B **66**, 245204 (2002).
[31] J. G. Lonnemann, E. P. Rugeramigabo, M. Oestreich, and J. Hübner, Phys. Rev. B **96**, 045201 (2017).
[32] K. V. Kavokin, Phys. Rev. B **64**, 075305 (2001).
[33] C. Herring and M. Flicker, Phys. Rev. **134**, A362 (1964).
[34] R. I. Dzhioev, V. L. Korenev, I. A. Merkulov, B. P. Zakharchenya, D. Gammon, A. L. Efros, and D. S. Katzer, Phys. Rev. Lett. **88**, 256801 (2002).
[35] G. Dresselhauss, Phys. Rev. **100**, 580 (1955).
[36] M. Cardona, N. E. Christensen, and G. Fasol, Phys. Rev. B **38**, 1806 (1988).
[37] F. Passmann, S. Anghel, T. Tischler, A. V. Poshakinskiy, S. A. Tarasenko, G. Karczewski, T. Wojtowicz, A. D. Bristow, and M. Betz, Phys. Rev. B **97**, 201413(R) (2018).
[38] C. Rice, D. Wolverson, A. Moskalenko, S. J. Bending, G. Karczewski, and T. Wojtowicz, Phys. Rev. B **87**, 121304(R) (2013).
[39] Note that the sample temperature can be significantly higher than the measured one since we are using a cold finger cryostat.
[40] See Ref. [6] and references therein.
[41] H. Ohadi, Y. del Valle-Inclan Redondo, A. Dreismann, Y. G. Rubo, F. Pinsker, S. I. Tsintzos, Z. Hatzopoulos, P. G. Savvidis, and J. J. Baumberg, Phys. Rev. Lett. **116**, 106403 (2016).
[42] R. M. Kroeze, Y. Guo, V. D. Vaidya, J. Keeling, and B. L. Lev, Phys. Rev. Lett. **121**, 163601 (2018).